LDPC-Coded MIMO Optical Communication Over the Atmospheric Turbulence Channel

Ivan B. Djordjevic, *Member, IEEE*, Stojan Denic, *Member, IEEE*, Jaime Anguita, *Member, IEEE*, Bane Vasic, *Senior Member, IEEE*, and Mark A. Neifeld, *Member, IEEE*

***Abstract*—In this paper, coded multiple-input–multiple-output (MIMO) communication schemes for data transmission over the optical atmospheric turbulence channels are studied. Two strategies are proposed and compared. The first is based on repetition coding, and the second on space–time (ST) coding. Both approaches employ low-density parity-check (LDPC) codes. The LDPC codes are designed using the concept of pairwise balanced design (PBD), balanced incomplete block design (BIBBD), and block–circulant (array) codes. To improve the spectral efficiency, we employ a bit-interleaved (BI) LDPC-coded modulation based on the pulse amplitude modulation (PAM). A better bit error rate (BER) performance is achieved by the iteration of extrinsic information between a demapper and LDPC decoder. The simulations show that the LDPC-coded MIMO schemes can operate under a strong atmospheric turbulence and at the same time provide excellent coding gains compared with the transmission of uncoded data. To verify the efficiency of the proposed coding schemes, achievable information rates are computed when the turbulence is modeled by a gamma–gamma distribution.**

***Index Terms*—Atmospheric turbulence, direct detection, free-space optical (FSO) communications, low-density parity-check (LDPC) codes, space–time (ST) coding.**

I. Introduction

FREE-SPACE optical (FSO) communications has recently received a significant attention as a possible alternative to conventional radio-frequency (RF)/microwave links for solving bottleneck connectivity problems in hybrid communication networks [1]. FSO communications also represents a promising technology to integrate a variety of interfaces and network elements. However, to exploit all potentials of FSO communication systems, the designers have to overcome some of the major challenges related to the optical wave propagation through the atmosphere. Namely, an optical wave propagating through the air experiences fluctuations in amplitude and phase due to atmospheric turbulence [1]–[7]. This intensity fluctuation, also known as scintillation, is one of the most important factors degrading the performance of an FSO communication link, even under the clear sky conditions.

Manuscript received June 2, 2007; revised December 3, 2007. This work was supported in part by the National Science Foundation (NSF) under Grant IHCS 0725405. Part of this paper was presented at the IEEE Global Communications Conference (Globecom), Washington, DC, November 26–30, 2007.

The authors are with the Department of Electrical and Computer Engineering, University of Arizona, Tucson, AZ 85721 USA (e-mail: ivan@ece.arizona.edu).

Color versions of one or more of the figures in this paper are available online at http://ieeexplore.ieee.org.

Digital Object Identifier 10.1109/JLT.2007.916514

The performance of FSO communication systems can be improved by using MIMO communication techniques. In the case of FSO communications, the MIMO concept is realized by employing *multiple optical sources at the transmitter side and multiple detectors at the receiver side*. In this paper, two scenarios, both employing low-density parity-check (LDPC) codes, are studied: 1) repetition multiple-input–multiple-output (MIMO) and 2) space–time coding [8]–[10]. Although this concept is analogous to wireless MIMO concept, the underlying physics is different, and optimal and suboptimal configurations for this channel are needed. In several recent publications, the MIMO scheme alone [2], [3] and its concatenation with different coding techniques [6] were studied assuming an ideal photon-counting receiver (the recent article [7] is an exception). In [6], we show that LDPC-coded repetition MIMO with pulse-position modulation is an excellent candidate, capable of enabling the communication over the strong atmospheric turbulence channels.

The goal of this paper is twofold: 1) to study different techniques for coded FSO MIMO communication, and 2) to evaluate the performance of proposed techniques in terms of the achievable information rates and the channel capacity. Two types of information theoretic bounds are determined: 1) the independent identically distributed (i.i.d.) channel capacity of the MIMO optical atmospheric channels using an approach proposed by Ungerboeck in [11], and 2) the MIMO achievable information rates using Telatar's approach found in [12]. The atmospheric optical channel is modeled by adopting the gamma–gamma probability density function due to Al-Habash *et al.* [4], which is valid for a wide range of turbulence strengths. Photodetection is assumed to be *nonideal*.

Further, we study two approaches as possible candidates to achieve these theoretical limits. The first approach is based on the LDPC-coded repetition MIMO principle. The second is based on the LDPC space–time (ST) coding MIMO scheme. The LDPC codes employed in this paper are designed using the combinatorial objects known as balanced incomplete block designs (BIBDs), and pairwise balanced designs (PBDs) [13], accompanied by block-circulant (array) codes [16], [17]. Both schemes are able to operate under strong atmospheric turbulence and provide excellent coding gains.

To improve the spectral efficiency of proposed schemes, we employed a bit-interleaved (BI) LDPC-coded modulation based on the pulse amplitude modulation (PAM). In order to improve bit error rate (BER) performance, we iterate the extrinsic log–likelihood ratios (LLRs) between *a posterior probability* (APP) demapper and LDPC decoder. The selection

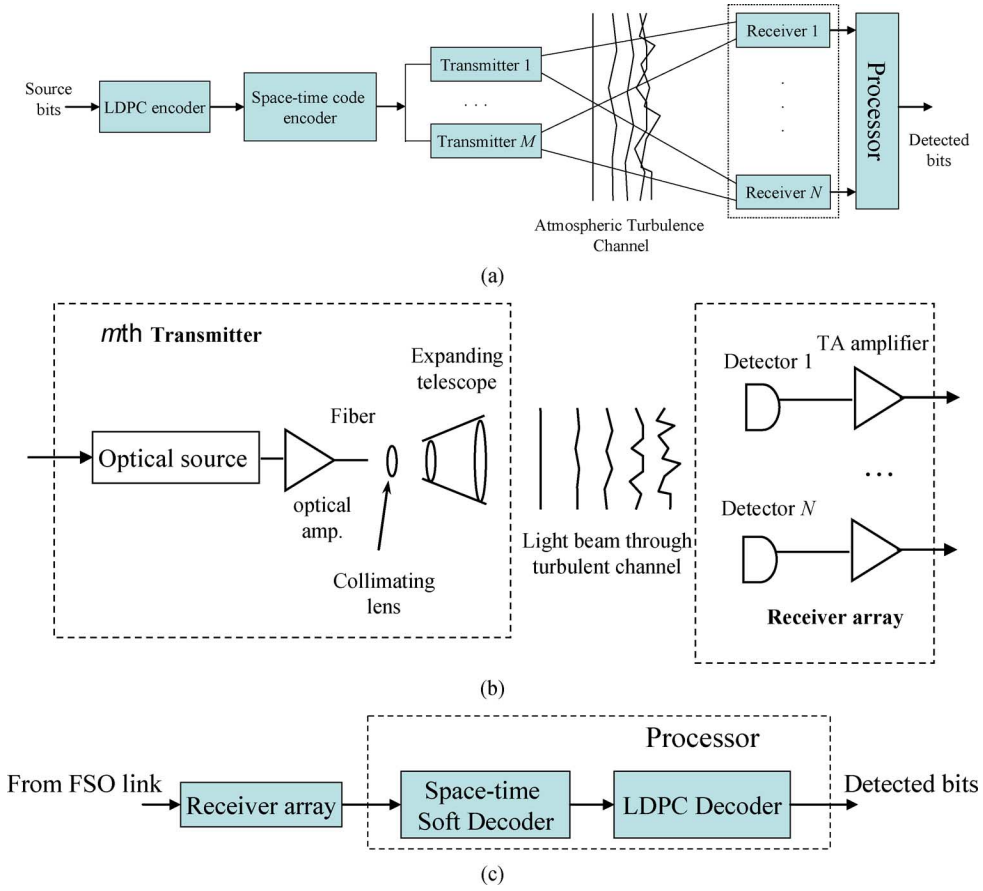

Fig. 1. (a) Atmospheric optical LDPC-coded MIMO system with ST block codes, (b) mth transmitter and receiver array configurations, and (c) processor configuration.

of LDPC codes suitable for iterative demmaping decoding is performed by the use of extrinsic information transfer (EXIT) charts [15]. To facilitate the implementation at high speeds, *structured* LDPC codes are employed in simulations.

This paper is organized as follows. The LDPC-coded MIMO strategy suitable for the FSO communication is explained in Section II. The achievable information rates, for the strategy described in Section II, are reported in Section III. The strategy of a BI LDPC-coded modulation, suitable to improve the spectral efficiency of MIMO FSO systems, is explained in Section IV. The convergence behavior is studied in Section IV-A. LDPC codes suitable for iterative demapping decoding selected by the EXIT chart analysis, are described in Section V. The simulation results are given in Section VI. Finally, Section VII summarizes the contributions.

II. LDPC-Coded MIMO Concept and ST Coding

A. Communication System

A block diagram of the proposed MIMO scheme is shown in Fig. 1. M optical sources are all pointed toward the distant array of N photodetectors using an expanding telescope. We assume that the beam spots on the receiver side are sufficiently wide to illuminate a whole photodetector array. This approach might help in simplifying the transmitter–receiver pointing problem. We further assume that the receiver's implementation is based on a positive–intrinsic–negative (p.i.n.) photodetector in a transimpedance amplifier (TA) configuration. In the case of the *repetition* MIMO, the nth photodetector output scheme can be represented by

$$y_n(l) = x(l)\sum_{m=1}^{M} I'_{nm} + z_n(l), \quad n = 1,\ldots,N, \qquad x(l) \in \{0, A\} \tag{1}$$

where A denotes the intensity of the pulse in the absence of scintillation, and $x(l)$ denotes data symbol at the lth time slot. I'_{nm} represents the intensity channel coefficient between the nth photodetector ($n = 1,2,\ldots,N$) and the mth ($m = 1,2,\ldots,M$) optical source, which is described by the gamma–gamma probability density function (pdf) [4]

$$f(I') = \frac{2(\alpha\beta)^{(\alpha+\beta)/2}}{\Gamma(\alpha)\Gamma(\beta)} I'^{(\alpha+\beta)/2-1} K_{\alpha-\beta}\left(2\sqrt{\alpha\beta\, I'}\right), \quad I' > 0 \tag{2}$$

where I' is the signal intensity, $\Gamma(\cdot)$ is the gamma function, and $K_{\alpha-\beta}(\cdot)$ is the modified Bessel function of the second kind and $\alpha - \beta$ order. α and β are the pdf parameters describing the

scintillation experienced by plane waves, and in the case of zero-inner scale are given by [4]

$$\alpha = \left\{ \exp\left[\frac{0.49\sigma_R^2}{(1+1.11\sigma_R^{12/5})^{7/6}} \right] - 1 \right\}^{-1}$$
$$\beta = \left\{ \exp\left[\frac{0.51\sigma_R^2}{(1+0.69\sigma_R^{12/5})^{5/6}} \right] - 1 \right\}^{-1} \quad (3)$$

where σ_R^2 is the Rytov variance given by

$$\sigma_R^2 = 1.23\, C_n^2\, k^{7/6} L^{11/6}. \quad (4)$$

In (4), $k = 2\pi/\lambda$ is the optical wave number, L is the propagation distance, and C_n^2 is the refractive index structure parameter, which we assume to be constant for horizontal paths. The optical sources and photodetectors are positioned in such a way that different transmitted symbols experience different atmospheric turbulence conditions. z_n denotes the nth receiver TA thermal noise that is modeled as a zero-mean Gaussian process with double-side power spectral density $N_0/2$.

B. Transmitter

We assume an ON–OFF keying (OOK) transmission over the atmospheric turbulence channel using incoherent light sources and direct detection. The information bearing signal is LDPC encoded. An ST encoder accepts K encoded bits x_k ($k = 1, 2, \ldots, K$) from an LDPC encoder. The ST encoder maps the input bits into the $T \times M$ matrix $\boldsymbol{O}$, whose entries are chosen from $\{x_1, x_2, \ldots, x_K, \overline{x}_1, \overline{x}_2, \ldots, \overline{x}_K\}$, so that the separation of decision statistics is possible at the receiver side, as shown later in (9) and (9a). T denotes the number of channel uses required to transmit K input bits. Notice that case $K = T = M = 2$ (M is the number of optical sources introduced in Section II-A)

$$\boldsymbol{O} = \begin{bmatrix} x_1 & x_2 \\ x_2 & \overline{x}_1 \end{bmatrix}$$

corresponds to the Alamouti-like ST code [9]. Here, $\overline{x}_i = 1 - x_i$ denotes the binary complement of x_i.

C. Repetition MIMO Versus ST Codes

As explained in [10], a fundamental difference between the wireless ST codes and ST codes for FSO communications with intensity modulation/direct detection (IM/DD) is that the latter employs nonnegative real/unipolar signals rather than complex/bipolar. That is why in IM/DD schemes $E(x_k) \neq 0$ so that the received power (observed in the electrical domain, after the photodetector), in a back-to-back configuration (in the absence of scintillation), is different for the repetition MIMO and ST codes. The total received power in repetition MIMO is determined by $E\left[(Mx)^2\right] = M^2 E\left(x^2\right) = M^2 \cdot A^2/2$, where $E[\cdot]$ is the operator of ensemble averaging, and $x \in \{0, A\}$. On the other hand, the total received power in MIMO ST coding, per one photodetector, is determined by

$$E\left[\left(\sum_{m=1}^{M} x_m\right)^2\right] = E\left[\sum_{m=1}^{M} x_i^2 + 2\sum_{m}\sum_{m'>m} x_m x_{m'}\right]$$
$$= ME\left(x^2\right) + M\left(M-1\right)E^2(x)$$
$$= \frac{1}{2}\left(M^2 + M\right)\cdot\frac{A^2}{2}.$$

Therefore, for the same transmitted power, the received power per photododetector for repetition MIMO is $2M/(M+1)$ times larger. Therefore, we can impose two different comparison criteria: 1) to keep the received power upon photodetection, in the back-to-back configuration, constant, or 2) to keep transmitted power (observed in electrical domain) constant.

D. Receiver

The received power (in electrical domain) per photodetector, for repetition MIMO transmission, is given by

$$E\left(y_n^2\right) = E\left[\left(x\sum_{m=1}^{M} I_{nm}\right)^2\right] = E\left[\left(\sum_{m=1}^{M} I_{nm}\right)^2 x^2\right]$$
$$= E\left(\sum_{m=1}^{M} I_{nm}^2 + 2\sum_{m}\sum_{m'>m} I_{nm} I_{nm'}\right) E\left(x^2\right)$$
$$= \left[ME\left(I^2\right) + M\left(M-1\right)E\left[I\right]^2\right]\frac{A^2}{2}. \quad (5)$$

This equation is used later in Sections III, IV, and VI to determine the electrical signal-to-noise ratio (SNR), and to determine the power spectral density N_0 from given SNR needed in the calculation of LLRs in (6).

Assuming that the receiver TA thermal noise is white Gaussian with a double-side power spectral density $N_0/2$, the LLR of a symbol $x(l)$ (at the lth time slot) for a binary repetition MIMO transmission is determined by

$$L\left(x\left(l\right)\right)$$
$$= \log\left\{ \prod_{n=1}^{N} \frac{\frac{1}{\sqrt{2\pi}\sqrt{\frac{N_0}{2}}} \exp\left[-\frac{y_n(l)^2}{\frac{2N_0}{2}} \right]}{\frac{1}{\sqrt{2\pi}\sqrt{\frac{N_0}{2}}} \exp\left[-\frac{\left(y_n(l) - \sum_{m=1}^{M} I_{nm}\right)^2}{N_0} \right]} \right\}$$
$$= \sum_{n=1}^{N} \left\{ -\frac{y_n(l)^2}{N_0} + \frac{\left(y_n(l) - \sum_{m=1}^{M} I_{nm}\right)^2}{N_0} \right\}. \quad (6)$$

In the calculations of LLRs in (6), we assumed that the channel state information (CSI), denoted by I_{nm}, is known to the receiver, but not to the transmitter.

When the ST coding is used, it can easily be verified (by using $x_i^2 = x_i$ and $\overline{x}_i x_i = 0$) that for FSO systems ST codes from orthogonal designs [8] do not satisfy the *orthogonality property* $\det\left(OO^T\right) = \left[\sum_i x_i^2\right]^n$. Nevertheless, the separation of decision statistics can be achieved, when the complements are properly chosen so that a simple APP ST decoder still exists. Note that, given the lack of orthogonality, $\boldsymbol{O}$ is not optimum. For the ST-coded MIMO scheme, the FSO channel can be described by

$$\begin{aligned}\boldsymbol{y} &= \begin{bmatrix} y_{11} & y_{21} & \cdots & y_{N1} \\ \cdots & \cdots & \cdots & \cdots \\ y_{1T} & y_{2T} & \cdots & y_{NT} \end{bmatrix} \\ &= \boldsymbol{O}\begin{bmatrix} I_{11} & I_{21} & \cdots & I_{N1} \\ \cdots & \cdots & \cdots & \cdots \\ I_{1M} & I_{2M} & \cdots & I_{NM} \end{bmatrix} + \begin{bmatrix} z_{11} & z_{21} & \cdots & z_{N1} \\ \cdots & \cdots & \cdots & \cdots \\ z_{1T} & z_{2T} & \cdots & z_{NT} \end{bmatrix}\end{aligned} \tag{7}$$

so that APP of x_k can be written as

$$\Pr\left(x_k|\boldsymbol{y}\right) = C f_k\left(x_k, \boldsymbol{y}\right)\Pr\left(x_k\right) \tag{8}$$

where C is a constant and $f_k(x_k, \boldsymbol{y})$ is a function independent of other symbols (different from x_k). For example, for ST code $K = T = M = 4$ with an encoder mapper

$$\boldsymbol{O} = \begin{bmatrix} x_1 & x_2 & x_3 & x_4 \\ \overline{x}_2 & x_1 & \overline{x}_4 & x_3 \\ \overline{x}_3 & x_4 & x_1 & \overline{x}_2 \\ \overline{x}_4 & \overline{x}_3 & x_2 & x_1 \end{bmatrix}$$

and N photodetectors, the LLR of x_k defined as

$$L\left(x_k\right) = \sum_{n=1}^{N} \log\left[\frac{p\left(x_k = 0|\boldsymbol{y}_n\right)}{p\left(x_k = 1|\boldsymbol{y}_n\right)}\right], \quad \boldsymbol{y}_n = \left[y_{n1} \;\; y_{n2} \;\; y_{n3} \;\; y_{n4}\right]^T$$

can be calculated by

$$L\left(x_k\right) = \sum_{n=1}^{N}\left[\frac{\left(\tilde{x}_k - 1\right)^2}{N_0} + \frac{I_{n1}^2 + I_{n2}^2 + I_{n3}^2 + I_{n4}^2 - 1}{N_0} - \frac{\tilde{x}_k^2}{N_0}\right], \quad k = 1, \ldots, 4 \tag{9}$$

where (9a), shown at the bottom of the page, holds. In calculating LLRs in (9), again, we assumed that CSI is known at the receiver side. Notice that even in a regular OOK, the CSI should be known to the receiver so that the decision threshold can be set up properly. The LLRs calculated in ST soft decoder [e.g., (9)] are forwarded to the LDPC decoder realized using an efficient implementation of sum-product algorithm. To derive (9), we used the maximum-likelihood (ML) detection rule as a starting point. Let $\boldsymbol{y}_n$ represent the nth column of $\boldsymbol{y}$ in (7), and $\boldsymbol{x}$ represent the sequence of transmitted bits $\boldsymbol{x} = [x_1 x_2 x_3 x_4]^T$. The ML detection rule of the nth receiver can be formulated as follows: chose the estimate of $\boldsymbol{x}$ so that $\log[p(\boldsymbol{y}_n|\boldsymbol{x})]$ is maximum. The $\log[p(\boldsymbol{y}_n|\boldsymbol{x})]$ can be obtained by

$$\begin{aligned}\log\left[p\left(y_n|x\right)\right] = &-\frac{\left[y_{n1} - \left(x_1 I_{n1} + x_2 I_{n2} + x_3 I_{n3} + x_4 I_{n4}\right)\right]^2}{N_0} \\ &- \frac{\left[y_{n2} - \left(\overline{x}_2 I_{n1} + x_1 I_{n2} + \overline{x}_4 I_{n3} + x_3 I_{n4}\right)\right]^2}{N_0} \\ &- \frac{\left[y_{n3} - \left(\overline{x}_3 I_{n1} + x_4 I_{n2} + x_1 I_{n3} + \overline{x}_2 I_{n4}\right)\right]^2}{N_0} \\ &- \frac{\left[y_{n4} - \left(\overline{x}_4 I_{n1} + \overline{x}_3 I_{n2} + x_2 I_{n3} + x_1 I_{n4}\right)\right]^2}{N_0}.\end{aligned}$$

By using $x_k^2 = x_k$ and $\overline{x}_k = 1 - x_k$, we were able to separate decisions for x_k ($k = 1, \ldots, 4$), and derive (9).

The received power per photodetector (assuming $K = T = M$ and ST coding) is given by

$$\begin{aligned}E\left(y_n^2\right) &= E\left[\left(\sum_{m=1}^{M} I_{nm} x_m\right)^2\right] \\ &= E\left(\sum_{m=1}^{M} I_{nm}^2 x_m^2 + 2\sum_{m}\sum_{m'>m} I_{nm} I_{nm'} x_m x_{m'}\right) \\ &= \sum_{m=1}^{M} E\left(I_{nm}^2\right) E\left\{x_m^2\right\} \\ &\quad + 2\sum_{m}\sum_{m'>m} E\left(I_{nm}\right) E\left(I_{nm'}\right) E\left\{x_m\right\} E\left\{x_{m'}\right\} \\ &= \left\{M E\left(I^2\right) + \frac{1}{2} M\left(M-1\right) E\left[I\right]^2\right\} E\left(x^2\right).\end{aligned} \tag{10}$$

Notice that the power efficiency of OOK-based MIMO is different from that of wireless communication phase-shift keying (PSK) MIMO because $E[x] \neq 0$, and a part of the energy is used for transmission of the second term in (5) and (10). Notice that the second term in (5) is a useful term because repletion MIMO is used, while the second term in (10), in the case of ST coded MIMO, is in fact the interference term. To keep the total output power (observed in electrical domain) fixed, the parameter A is to be properly chosen (and it is different in repetition MIMO and ST-coded MIMO). For gamma–gamma distribution

$$\begin{aligned}\tilde{x}_1 &= \sum_{n=1}^{N}\left(I_{n1}y_{n1} + I_{n2}y_{n2} + I_{n3}y_{n3} + I_{n4}y_{n4} - I_{n1}I_{n2} - I_{n2}I_{n3} - I_{n1}I_{n3} - I_{n3}I_{n4} - I_{n1}I_{n4} - I_{n2}I_{n4}\right) \\ \tilde{x}_2 &= \sum_{n=1}^{N}\left(I_{n2}y_{n1} - I_{n1}y_{n2} - I_{n4}y_{n3} + I_{n3}y_4 + I_{n1}^2 + I_{n1}I_{n3} + I_{n1}I_{n4} + I_{n4}^2 - I_{n1}I_{n3} - I_{n2}I_{n3}\right) \\ \tilde{x}_3 &= \sum_{n=1}^{N}\left(I_{n3}y_{n1} + I_{n4}y_{n2} - I_{n1}y_{n3} - I_{n2}y_{n4} - I_{n1}I_{n4} - I_{n3}I_{n4} + I_{n1}^2 + I_{n1}I_{n4} + I_{n1}I_{n2} + I_{n2}^2\right) \\ \tilde{x}_4 &= \sum_{n=1}^{N}\left(I_{n4}y_{n1} - I_{n3}y_{n2} + I_{n2}y_{n3} - I_{n1}y_{n4} + I_{n1}I_{n3} + I_{n3}^2 - I_{n1}I_{n2} - I_{n2}I_{n4} + I_{n1}^2 + I_{n1}I_{n2}\right).\end{aligned} \tag{9a}$$

[4], $E[I]=1$, and $E[I^2]$ is related to the scintillation index (SI) by [4]

$$\sigma_I^2=\frac{E\left[I^2\right]}{E\left[I\right]^2}-1=\frac{1}{\alpha}+\frac{1}{\beta}+\frac{1}{\alpha\beta} \tag{11}$$

where α and β have already been introduced in (3).

III. Achievable Rate Studies

In this section, we turn our attention to the calculation of achievable information rates. Achievable information rate represents a lower bound on the channel capacity, i.e., if the coding rate is smaller than the achievable rate the BER can be made arbitrarily close to zero. This is the best we can do at this moment because the channel capacity of additive noise channels subject to the positive input and the power constraint is not known. Next, we treat two situations: first, when the Q-ary PAM transmission is used, and the second, when the biased Gaussian input is assumed.

The MIMO i.i.d capacity R is computed (also known as achievable information rate) for Q-ary PAM by using Ungerboeck 's approach [11, eq. (5)]

$$R=\log_2 Q-\underset{I_n}{E}\ \underset{y|I_n}{E}\left\{\log_2\left[1+\sum_{q=1}^{Q-1}\exp\left(-\sum_{n=1}^{N}\frac{(Y_{n,q}-qAI_n)^2-Y_{n,q=0}^2}{N_0}\right)\right]\right\} \tag{12}$$

where $I_n=\sum_{m=1}^{M}I_{n,m}$, and $Y_{n,q}$ denotes the nth receiver response to the qth symbol (other parameters are introduced earlier). Notice that ensemble averaging is to be done for different channel conditions (the averaging done with respect to I_n) and for different thermal noise realizations (the averaging is done with respect to $\boldsymbol{y}|I_n$) by using Monte Carlo simulations. Ungerboeck derived the i.i.d. capacity formula in the context of multiamplitude/multiphase signals, and as such is directly applicable here. However, there are two important differences: 1) in IM/DD systems, we are concerned with nonnegative real signals rather than complex, and 2) we need to perform the additional averaging compared to [11], which is the averaging with respect to the channel conditions (scintillation). To derive (12), we had to apply the channel capacity formula for a discrete memoryless channel (see [19, eq. (7.1-18)])

$$C=\max y_{P(q)}\sum_{q=0}^{Q-1}\sum_{n=1}^{N}\int_{-\infty}^{\infty}p\left(Y_{n,q}|q\right)P\left(q\right)\times\log_2\left(\frac{p(Y_{n,q}|q)P(q)}{\sum_{i=0}^{Q-1}p(Y_{n,i}|i)P(i)}\right)dY_{n,q}$$

where

$$p(Y_{n,q})\frac{1}{\sqrt{2\pi}\sqrt{\frac{N_0}{2}}}\exp\left[-\frac{(Y_{n,q}-qAI_n)^2}{N_0}\right]$$

and assuming the equiprobable transmission $P(q)=1/Q$.

In Fig. 2(a), we plotted the i.i.d. capacity for binary transmission in strong turbulence regime ($\sigma_R=3.0$) for different number of optical sources, and photodetectors, against the electrical SNR ratio per photodetector, denoted by E/N_0, in the presence of scintillation. A slightly better improvement is obtained by increasing the number of optical sources than by increasing the number of photodetectors. The MIMO FSO systems with $M=N=2$, $M=4$, $N=1$, are comparable. In Fig. 2(b), we plotted the i.i.d. capacity for the Q-ary PAM. A significant i.i.d. channel capacity improvement is obtained by employing the MIMO concept relative to the single-source–single-detector technique.

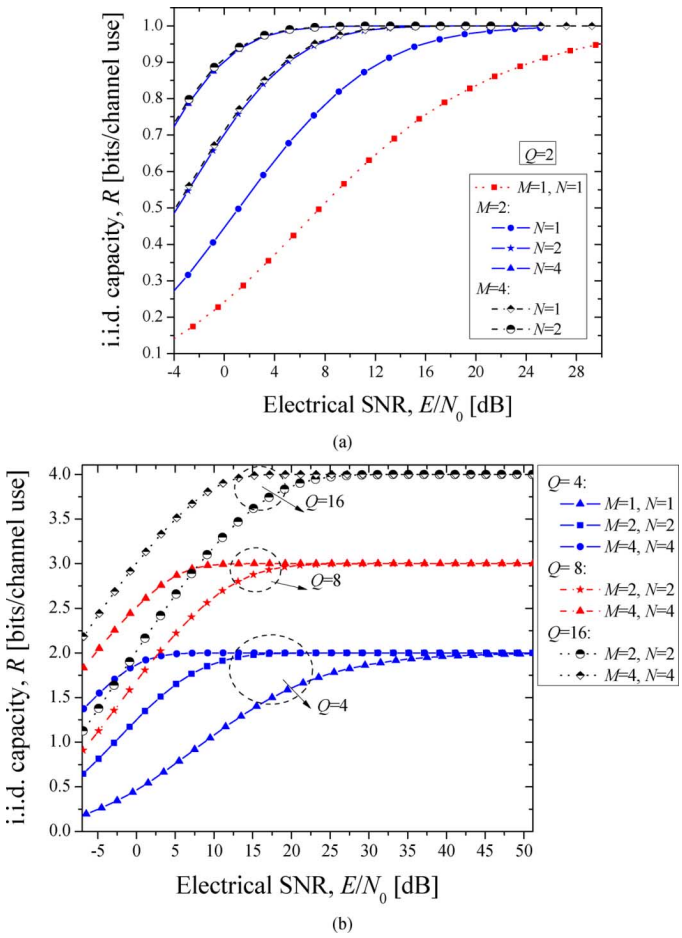

Fig. 2. The i.i.d channel capacity for different numbers of optical sources (M) and photodetectors (N) in strong turbulence regime ($\sigma_R=3.0$, $\alpha=5.485$, and $\beta=1.1156$) for (a) binary transmission and (b) Q-ary PAM.

The biased-Gaussian MIMO information rate can be calculated using the concept introduced by Telatar in [12] as follows:

$$R=\frac{1}{2}E\left[\log_2\det\left(\boldsymbol{I}_N+\frac{E_s}{N_0}\boldsymbol{H}\boldsymbol{H}^T\right)\right] \tag{13}$$

where $\boldsymbol{I}_N$ denotes $N\times N$ identity matrix, and $\boldsymbol{H}$ denotes the FSO channel matrix. Because a negative signal cannot be transmitted over an IM/DD system, the bias 3σ, with σ being the standard deviation of a Gaussian source, is added. Notice that factor $1/2$ in (13) comes from the fact that complex signals were considered in [12], while the signals here are real and nonnegative. In both cases, the single polarization transmission is assumed. The information rate in (13) is calculated by Monte

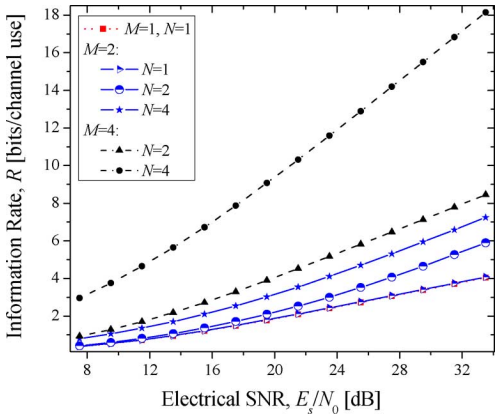

Fig. 3. MIMO achievable information rates for different number of lasers (M) and photodetectors (N) in strong turbulence regime ($\sigma_R = 3.0$, $\alpha = 5.485$, and $\beta = 1.1156$).

Carlo simulations and the information rates (in bits/channel use) are shown in Fig. 3 against electrical average symbol energy (E_s) to power spectral density (N_0) ratio. A significant spectral efficiency improvement is possible by using the multilevel schemes. One such scheme based on a Q-ary PAM is considered in Section IV.

IV. BI LDPC-Coded PAM

The block scheme of the BI LDPC-coded PAM technique, for a repetition MIMO transmission, is shown in Fig. 4. The source bit stream is encoded using an (n,k) LDPC code of the code rate $r = k/n$ (k being the number of information bits and n being the codeword length). The $l \times L$ block interleaver (L is an integer multiple of the codeword length n) collects l codewords written rowwise. The mapper accepts l bits at a time from the interleaver columnwise and determines the corresponding symbol for the Q-ary ($Q = 2^l$) PAM signaling using a *Gray mapping* rule. The number of columns in block interlever L is determined by a data rate and temporal correlation of the channel. We assume that the interleaver size is sufficient to overcome a temporal correlation of the channel, so that the channel samples are uncorrelated. The basis function is given by

$$\phi_{\mathrm{PAM}}(t) = \frac{1}{\sqrt{T}}\mathrm{rect}\left(\frac{t}{T}\right), \quad \mathrm{rect}(t) = \begin{cases} 1, & 0 \le t < 1 \\ 0, & \text{otherwise} \end{cases}$$

while the signal constellation points by $A_q = qd$ ($q = 0, 1, \ldots, Q-1$), where d is the separation between two neighboring points.

The average symbol energy is given by

$$E_s = \frac{(Q-1)(2Q-1)}{6}d^2$$

and it is related to the bit energy E_{b} by $E_s = E_{\mathrm{b}} \log_2 Q$. With this BI LDPC-coded modulation scheme, the neighboring information bits from the same source are allocated into different PAM symbols. The outputs of the N receivers in the repetition MIMO, denoted as y_n ($n = 1, 2, \ldots, N$), are processed to determine the symbol reliabilities (LLRs) by

$$\begin{aligned} &\lambda(q) \\ &= \log\left\{\frac{1}{\sqrt{2\pi}\sqrt{\frac{N_0}{2}}}\exp\left[-\frac{\left(y_n - \mathrm{map}(q)\, d \sum_{m=1}^{M} I_{nm}\right)^2}{N_0}\right]\right\} \\ &= -\sum_{n=1}^{N}\frac{\left(y_n - \mathrm{map}(q)\, d \sum_{m=1}^{M} I_{nm}\right)^2}{N_0} + \log\left(\frac{1}{\sqrt{2\pi}\sqrt{\frac{N_0}{2}}}\right), \\ &\qquad q = 0, 1, \ldots, Q-1 \end{aligned} \tag{14}$$

where $\mathrm{map}(q)$ denotes a corresponding mapping rule. The second term in the second line of (14) can be neglected in simulations because it is constant for all symbols. Further, denote by c_j the jth bit in an observed symbol q binary representation $\boldsymbol{c} = (c_1, c_2, \ldots, c_l)$. The bit reliabilities $L(c_j)$ are determined from symbol reliabilities by

$$L(c_i) = \log\frac{\sum_{c:c_i=0}\exp[\lambda(q)]\exp\left(\sum_{c:c_j=0, j\neq i} L_a(c_j)\right)}{\sum_{c:c_i=1}\exp[\lambda(q)]\exp\left(\sum_{c:c_j=0, j\neq i} L_a(c_j)\right)} \tag{15}$$

and forwarded to the LDPC decoder. Therefore, the ith bit reliability is calculated as the logarithm of the ratio of a probability that $c_i = 0$ and probability that $c_i = 1$. In the nominator, the summation is done over all symbols q having 0 at the position i, while in the denominator, it is done over all symbols q having 1 at the position i. With $L_a(c_j)$, we denoted *a priori* information determined from the LDPC decoder extrinsic LLRs. The inner summation in (15) is done over all bits of symbol q, selected in the outer summation, for which $c_j = 0$, $j \neq i$. By iterating the extrinsic reliabilities between APP demapper and LDPC decoder, the overall BER performance can be improved. The hard decisions from the LDPC decoder are delivered to the end user. Once more, in calculations of the symbol LLRs in (14), we assumed that CSI is known at the receiver side.

Other multilevel schemes, such as those based on quadrature amplitude modulation (QAM) are also applicable. However, the use of an additional direct current (dc) bias is required because negative signals cannot be transmitted over an IM/DD system, and the power efficiency of such schemes is low.

A. Iterative Demapping and Decoding

To improve the BER performance, we perform the iteration of *extrinsic* information between APP PAM demapper and LDPC decoder. For a convergence behavior analysis, we perform the EXIT chart analysis. To determine the mutual information (MI) transfer characteristics of the demapper, we model *a priori* input LLR $L_{M,a}$ as a conditional Gaussian random variable [15]. The MI between the bit c in a codeword and corresponding input LLR ($L_{M,a}$) is determined numerically as explained in [15].

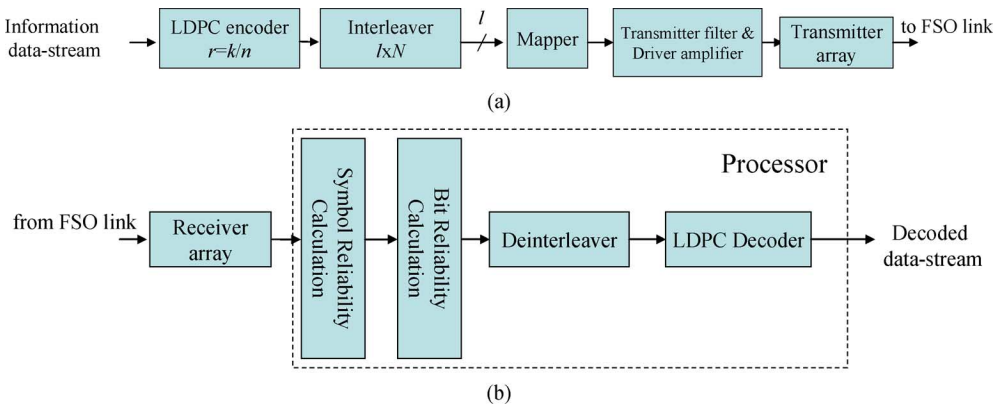

Fig. 4. Repetition MIMO BI LDPC-coded PAM (a) transmitter and (b) receiver configurations.

Similarly, the MI $I_{LM,e}$ between c and $L_{M,e}$ is calculated numerically, but with the pdf of c and $L_{M,e}$ determined form the histogram obtained by Monte Carlo simulation, as explained in [15]. By observing the $I_{LM,e}$ as a function of the MI of $I_{LM,a}$ and receiver SNR E/N_0 in decibels, the demapper EXIT characteristic (denoted as T_M) is given by

$$I_{L_{M,e}} = T_M\left(I_{L_{M,a}}, \frac{E}{N_0}\right).$$

The EXIT characteristic of the LDPC decoder (denoted by T_D) is defined in a similar fashion as

$$I_{L_{D,e}} = T_D\left(I_{L_{D,a}}\right).$$

The "turbo" demapping-based receiver operates by passing extrinsic LLRs between the demapper and LDPC decoder. The iterative process starts with an initial demapping, in which $L_{M,a}$ is set to zero having a consequence $I_{LM,a} = 0$. The demapper output LLRs described by

$$I_{L_{M,e}} = I_{L_{D,a}}$$

are fed to the LDPC decoder. The LDPC decoder output LLRs described by

$$I_{L_{D,e}} = I_{L_{M,a}}$$

are fed to the APP demapper. The iterative procedure is repeated until the convergence or the maximum number of iterations has been reached. This procedure is illustrated in Fig. 5, where the APP demapper and LDPC decoder EXIT charts are shown together on the same graph. The 4-PAM, 8-PAM, and 16-PAM are observed, as well as the natural and Gray mapping. The EXIT curves have different slopes for different mappings. The existence of "tunnel" between corresponding demapping and decoder curves indicates that the iteration between demapper and decoder will be successful. The smallest SNR at which the iterative scheme starts to converge is known as the threshold (pinch-off) limit [15]. The threshold limit in the case of 16-PAM [Fig. 5(b)] is about 8 dB worse as compared to 4-PAM [Fig. 5(a)].

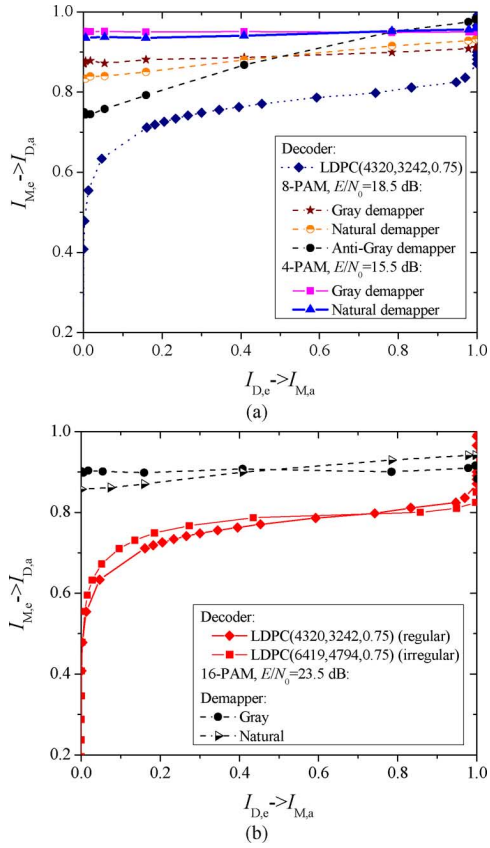

Fig. 5. EXIT chart for different PAM constellations: (a) 4-QAM and 8-PAM and (b) 16-PAM.

V. LDPC Codes

The communication techniques proposed in this paper assume the application of LDPC codes. In this section, the selection of *structured* LDPC codes suitable for iterative demapping decoding is considered. Three classes of LDPC codes are selected using the EXIT chart analysis from Section IV.

The first class is the class of girth-8 *regular* LDPC codes designed based on the concept of BIBDs [13]. The second class of the codes is the class of *irregular* girth-8 LDPC codes obtained from the combinatorial objects known as PBDs [13]. A PBD, denoted as PBD$(v, K, \{0, 1, \ldots, \lambda\})$, is a collection of subsets (also known as blocks) of a v-set V with a size of each

block $k_i \in K$ $(k_i \leq v)$, so that each pair of elements occurs in *at most* λ of the blocks. Notice that we have relaxed the constraint in the definition of the PBD from [13] by replacing the word *exact* with *at most*. The main purpose of this relaxation is to increase the number of possible PBDs that result in the LDPC codes of desired code rates. As an illustration, the following blocks $\{1,6,9\}$, $\{2,7,10\}$, $\{3,8,11\}$, $\{4,12\}$, $\{5,13\}$, $\{1,7,11\}$, $\{2,8,12\}$,$\{3,13\}$, $\{1,8,13\}$, $\{2,9\}$, $\{3,10\}$, $\{4,6,11\}$, $\{5,7,12\}$, $\{1,10\}$, $\{2,11\}$, $\{3,6,12\}$, $\{4,7,13\}$, $\{5,8,9\}$, $\{1,12\}$, $\{2,6,13\}$, $\{3,7,9\}$, $\{4,8,10\}$, and $\{5,11\}$ create a PBD$(13,\{2,3\},\{0,1\})$, with parameter $\lambda \leq 1$. By considering elements of blocks as the positions of ones in corresponding element-block incidence matrix, a parity-check matrix of an equivalent *irregular* LDPC code of girth-6 is obtained. To increase the girth to 8, certain blocks from a PBD are to be removed. The BIBD can be considered as a special class of PBDs in which all of the blocks are of the same size. The third-class of codes is class of block-circulant (BC) LDPC codes [16] (also known as array LDPC codes [17]) of girth-8. The parity check matrix of BC codes can be described as follows:

$$\boldsymbol{H} = \begin{bmatrix} P^{i_1} & P^{i_2} & P^{i_3} & \cdots & P^{i_q} \\ P^{i_q} & P^{i_1} & P^{i_2} & \cdots & P^{i_q-1} \\ \cdots & \cdots & \cdots & \cdots & \cdots \\ P^{i_q-r+2} & P^{i_q-r+3} & P^{i_q-r+4} & \cdots & P^{i_q-r+1} \end{bmatrix} \quad (16)$$

with P being the permutation matrix $P = (p_{ij})_{nxn}$, $p_{i,i+1} = p_{n,1} = 1$ (zero, otherwise). The exponents $i_1, i_2, \ldots, i_q$ in (16) are carefully chosen to avoid the cycles of length six in the corresponding bipartite graph of a parity-check matrix. For more details on BC codes, an interested reader is referred to [16].

VI. Simulation Results

The BER versus electrical SNR in the presence of scintillation (per photodetector), for a strong turbulence regime ($\sigma_R = 3.0, \alpha = 5.485$, and $\beta = 1.1156$), are shown in Fig. 6. The BER is shown for a different number of optical sources, and photodetectors, by employing an $(6419, 4794)$ irregular girth-6 LDPC code of a rate 0.747 designed using the concept of the PBD. The option 1) (see Section II-C) is used as comparison criterion. If the transmitted power observed in the electrical domain [option 2)] is to be used as a comparison criterion, the repetition MIMO curves are to be shifted by $10\log_{10}(2M/(M+1))$ decibels to the left. In simulations, in order to vary the SNR, the signal energy was kept constant while the electrical noise power spectral density was varied instead.

The Alamouti-like ST code performance is comparable to the repetition MIMO, while $T = 4$ ST performs worse than the corresponding repetition MIMO. The reason for such a behavior comes from the fact that we operate with nonnegative real signals rather than with complex, so that the ST codes from orthogonal designs [8], [9] are not optimal in an FSO channel. Moreover, the second term in (10) behaves as interference, while in repetition MIMO [see (5)] it is a useful signal. The LDPC-coded MIMO with Alamouti-like code $(M = 2)$ and $N = 4$ photodetectors provides about 20-dB improvement over LDPC-coded OOK with single optical source and single photodetector. Further performance improvements can be obtained by iterating between LDPC decoder and soft ST decoder at the expense of the increased decoding delay. Although a significant coding gain is obtained, from the channel capacity curves, it is obvious that we are still several decibels away from the channel capacity. This suggests that neither the coded repetition MIMO nor the wireless ST codes are channel capacity approaching techniques. In order to come closer to the channel capacity, novel ST codes taking the underlying FSO physics into account are needed, but still not known. One possible option would be the use of Bell Labs layered space–time architecture (BLAST) [14] to deal with interference from (10), in combination with long LDPC codes.

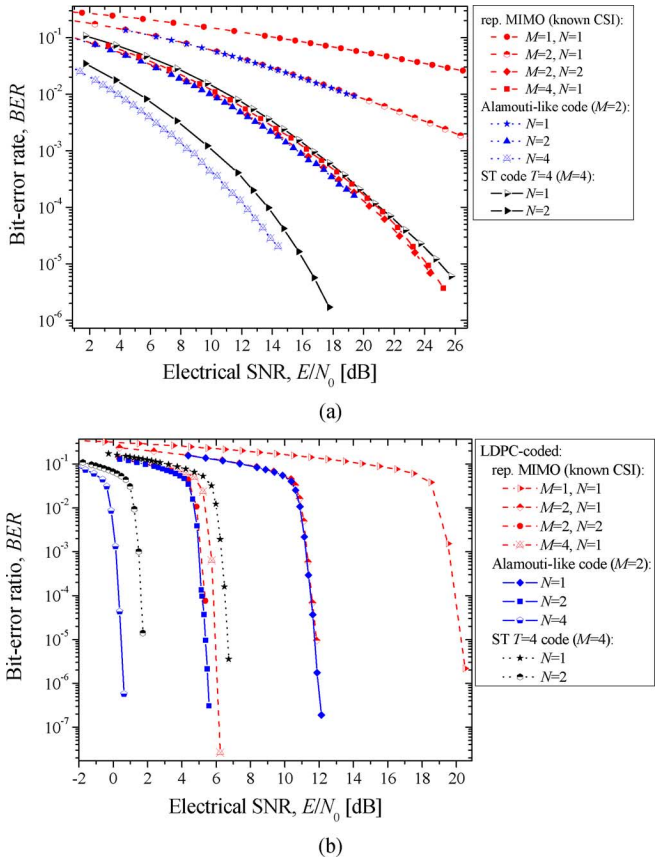

Fig. 6. BERs of binary LDPC$(6419, 4794)$-coded MIMO ST coding scheme against LDPC-coded repetition MIMO: (a) uncoded case and (b) coded case.

The results of simulations for BI LDPC$(6419, 4794)$-coded PAM are shown in Fig. 7 for different MIMO configurations and different number of signal constellation points employing the Gray mapping rule. Once more, although excellent BER performance improvement is obtained (about 23 dB for $M = N = 4$, $Q = 4$ over $M = N = 1$, $Q = 4$), there is still some space for improvement to come closer to the channel capacity, which was left for further research. The comparison for different component LDPC codes is given in Fig. 8. The scheme employing a girth-6 (g-6) irregular PBD-based LDPC code of rate 0.75 performs comparable to a girth-8 regular BC-LDPC code of the same rate. The scheme based on a girth-8 regular BIBD code of rate 0.81 performs worse than 0.75 codes. However, the difference is becoming less important as the constellation size grows.

Note that in the previous simulations, we assume that the channel is uncorrelated (see also [2], [3], and [5]–[7]). As we

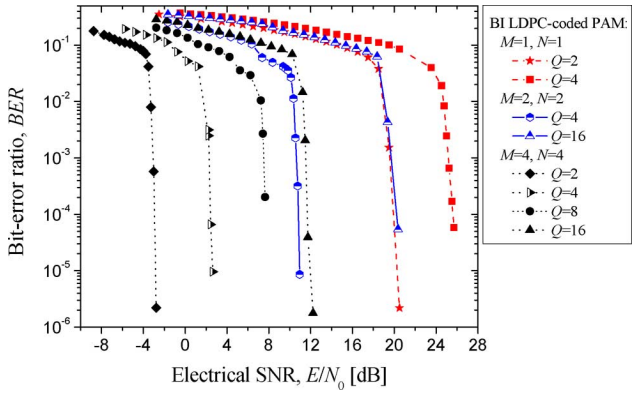

Fig. 7. BER performance of BI-LDPC$(6419, 4794)$-coded PAM with repetition MIMO.

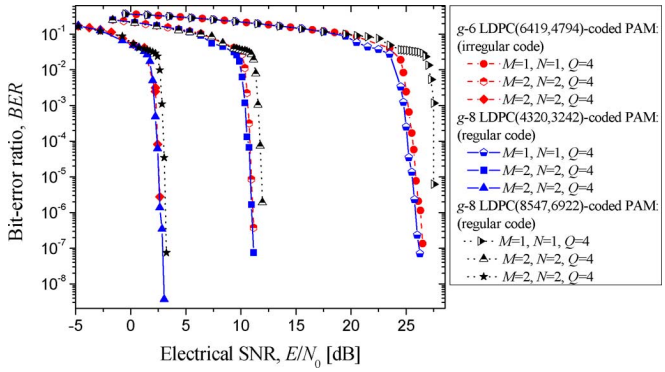

Fig. 8. BER performance of BI-LDPC-coded PAM with repetition MIMO for different LDPC component codes.

mentioned earlier, we assumed that a temporal correlation can be overcome by means of interleavers, and possibly by orthogonal frequency division multiplexing (OFDM) [18]. Unfortunately, the temporal correlation is difficult to simulate, especially under strong turbulence regimes (see [18]).

VII. Summary

In this paper, we consider achievable information rates for FSO MIMO transmission, and study two coded MIMO schemes as possible alternatives to achieve the channel capacity: 1) repetition MIMO scheme, and 2) ST-coding-based MIMO scheme. Both schemes employ LDPC codes. To facilitate the implementation at high speeds, we prefer the use of structured LDPC codes instead of random LDPC codes. The structured LDPC codes are designed using the following concepts: PBDs, BIBDs, and block-circulant (array) codes. To improve the BER performance, we allow the iteration of extrinsic information between demapper and LDPC decoder. For the convergence behavior of the iterative demapping decoding, EXIT chart analysis is performed. The BERs and achievable information rates are reported assuming a nonideal photodetection. To improve the spectral efficiency of coded MIMO schemes, we employed the concept of BI LDPC-coded modulation based on Q-ary PAM. The Alamouti-like-based LDPC-coded MIMO scheme with four photodetectors provides about 20-dB improvement over a single optical source/single photodetector scheme at a BER of 10^{-6}. Although excellent BER performance improvements, over an uncoded case with one light source and one photodetector, are obtained, from channel capacity studies, we can conclude that we are still several decibels away from the channel capacity curves. Novel ST coding approaches are needed that take the physics of a FSO channel into account, which is left for further research. Those approaches will enable us to come closer to the channel capacity.

References

[1] H. Willebrand and B. S. Ghuman, *Free-Space Optics: Enabling Optical Connectivity in Today's Networks*. Indianapolis, IN: Sams Publishing, 2002.

[2] S. G. Wilson, M. Brandt-Pearce, Q. Cao, and J. J. H. Leveque, III, "Free-space optical MIMO transmission with Q-ary PPM," *IEEE Trans. Comm.*, vol. 53, no. 8, pp. 1402–1412, Aug. 2005.

[3] S. G. Wilson, M. Brandt-Pearce, Q. Cao, and M. Baedke, "Optical repetition MIMO transmission with multipulse PPM," *IEEE J. Sel. Areas Comm.*, vol. 23, no. 9, pp. 1901–1910, Sep. 2005.

[4] M. A. Al-Habash, L. C. Andrews, and R. L. Phillips, "Mathematical model for the irradiance probability density function of a laser beam propagating through turbulent media," *Opt. Eng.*, vol. 40, pp. 1554–1562, 2001.

[5] J. A. Anguita, I. B. Djordjevic, M. A. Neifeld, and B. V. Vasic, "Shannon capacities and error–correction codes for optical atmospheric turbulent channels," *OSA J. Opt. Netw.*, vol. 4, pp. 586–601, Sep. 2005.

[6] I. B. Djordjevic, B. Vasic, and M. A. Neifeld, "Multilevel coding in free-space optical MIMO transmission with Q-ary PPM over the atmospheric turbulence channel," *IEEE Photon. Tehnol. Lett.*, vol. 18, no. 14, pp. 1491–1493, Jul. 2006.

[7] N. Cvijetic, S. G. Wilson, and M. Brandt-Pearce, "Receiver optimization in turbulent free-space optical MIMO channels with APDs and Q-ary PPM," *IEEE Photon. Tehnol. Lett.*, vol. 19, no. 2, pp. 1491–1493, Jan. 2007.

[8] V. Tarokh, H. Jafarkani, and A. R. Calderbank, "Space-time block codes from orthogonal designs," *IEEE Trans. Inf. Theory*, vol. 45, no. 5, pp. 1456–1467, Jul. 1999.

[9] S. M. Alamouti, "A simple transmit diversity technique for wireless communications," *IEEE J. Sel. Areas Commun.*, vol. 16, no. 8, pp. 1451–1458, Oct. 1998.

[10] K. Simon and V. A. Vilnrotter, "Alamouti-type space-time coding for free-space optical communication with direct detection," *IEEE Trans. Wireless Commun.*, vol. 4, no. 1, pp. 35–39, Jan. 2005.

[11] G. Ungerboeck, "Channel coding with multilevel/phase signals," *IEEE Trans. Inf. Theory*, vol. IT-28, no. 1, pp. 55–67, Jan. 1982.

[12] E. Telatar, "Capacity of multi-antena Gaussian channels," *Eur. Trans. Telecomm.*, vol. 10, no. 6, pp. 585–595, Nov./Dec. 1999.

[13] I. Anderson, *Combinatorial Designs and Tournaments*. Oxford, U.K.: Oxford Univ. Press, 1997.

[14] G. J. Foschini, "Layered space-time architecture for wireless communication in a fading environment when using multi-element antennas," *Bell Labs Tech. J.*, vol. 1, no. 2, pp. 41–59, 1996.

[15] S. ten Brink, "Designing iterative decoding schemes with the extrinsic information transfer chart," *AEÜ Int. J. Electron. Commun.*, vol. 54, pp. 389–398, Dec. 2000.

[16] O. Milenkovic, I. B. Djordjevic, and B. Vasic, "Block-circulant low-density parity-check codes for optical communication systems," *IEEE J. Sel. Topics Quantum Electron.*, vol. 10, no. 2, pp. 294–299, Mar./Apr. 2004.

[17] J. L. Fan, "Array codes as low-density parity-check codes," in *Proc. 2nd Int. Symp. Turbo Codes Related Topics*, Brest, France, Sep. 2000, pp. 543–546.

[18] I. B. Djordjevic, B. Vasic, and M. A. Neifeld, "LDPC coded OFDM over the atmospheric turbulence channel," *Opt. Express*, vol. 15, pp. 6332–6346, 2007.

[19] J. G. Proakis, *Digital Communications*. Boston, MA: McGraw-Hill, 2001.

Ivan B. Djordjevic (M'04) received the B.Sc., M.Sc., and Ph.D. degrees in electrical engineering from the University of Nis, Nis, Serbia, in 1994, 1997, and 1999, respectively.

Currently, he is an Assistant Professor of Electrical and Computer Engineering at the University of Arizona, Tucson. He was with the University of the West of England, Bristol, U.K., University of Bristol, Bristol, U.K., Tyco Telecommunications, Eatontown, NJ, and National Technical University of Athens, Athens, Greece. His current research interests include optical networks, error control coding, constrained coding, coded modulation, turbo equalization, OFDM, and quantum communications. He is author of more than 100 international publications.

Stojan Denic (S'04–M'06) received the B.Sc. and M.Sc. degrees in electrical engineering from the Faculty of Electronic Engineering, University of Nis, Nis, Serbia, in 1994 and 2001, respectively, and the Ph.D. degree from the School of Information Technology and Engineering, University of Ottawa, Ottawa, ON, Canada.

From 1996 to 2000, he was with the Telecom Serbia. Currently, he is a Research Assistant Professor at the Electrical and Computer Engineering Department, University of Arizona, Tucson. His research interests include information theory, communication over uncertain channels, control over communication channels, optical communications, and coding for wireless and digital recording channels.

Jaime Anguita (S'02–M'07) received the B.S. degree from Universidad Catolica, Santiago, Chile, in 1994 and the M.S. and Ph.D. degrees from the University of Arizona, Tucson, in 2004 and 2007, respectively, all in electrical engineering.

He worked for the European Southern Observatory and for a Chilean power distribution company. His research interests are optical communications, both free-space and fiber-based, channel characterization, modulation and error-control coding, and signal processing.

Dr. Anguita is a member of the Optical Society of America (OSA) and International Society for Optical Engineering (SPIE).

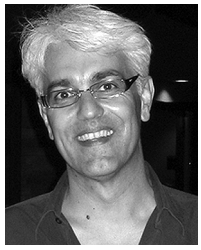

Bane Vasic (S'92–M'93–SM'02) received the B.Sc., M.Sc., and Ph.D. degrees in electrical engineering from the University of Nis, Nis, Serbia, in 1989, 1991, and 1994, respectively.

Currently, he is a Professor of Electrical and Computer Engineering and Mathematics at the University of Arizona, Tucson. Prior to this appointment, he was at Bell Laboratories. He authored a number of journal and conference articles and book chapters, and edited two books. His patents are implemented in Bell Lab chips. His research interests include coding theory, communication theory, constrained systems, and digital communications and recording.

Dr. Vasic is a Member of the Editorial Board of the IEEE TRANSACTIONS ON MAGNETICS, and was a Chair or Technical Program Chair for several workshops and conferences including: 2003 and 2007 IEEE Communication Theory Workshop (CTW), 2004 DIMACS Workgroup and Workshop on Theoretical Advances in Information Recording, 2004 LANL Workshop on Applications of Statistical Physics to Coding Theory, and 2006 Communication Theory Symposium within ICC.

Mark A. Neifeld (S'84–M'91) received the B.S.E.E. degree from the Georgia Institute of Technology, Atlanta, in 1985 and the M.S. and Ph.D. degrees in electrical engineering from the California Institute of Technology, Pasadena, in 1987 and 1991, respectively.

During the 1985–1986 academic year, he was also a member of the technical staff in the TRW Systems Engineering and Analysis Laboratory, Redondo Beach, CA. For one year, he held a postdoctoral position at the NASA Jet Propulsion Laboratories, Pasadena, CA, where he studied the application of parallel image processing techniques to problems in target recognition. In August 1991, he joined the faculty of the Department of Electrical and Computer Engineering, University of Arizona, Tucson. He is also a member of the faculty of the Optical Sciences Center at the University of Arizona and has coauthored more than 50 conference and journal papers in the areas of optical storage, parallel coding and signal processing, optoelectronic device simulation and CAD, computer generated holography, character recognition, neural networks, and optical processing systems. His thesis work focused on the use of parallel access optical memories for image pattern recognition. He presently directs the Optical Computing and Processing Laboratory within the ECE Department at the University of Arizona.

Dr. Neifeld serves as a Topical Editor for *Applied Optics*.